ISBN: 978-3-95450-227-1 ISSN: 2673-5490 doi:10.18429/JACoW-IPAC2022-MOPOST055

THE EIC RAPID CYCLING SYNCHROTRON DYNAMIC APERTURE OPTIMIZATION

H. Lovelace III*, C. Montag, V. Ranjbar, Brookhaven National Laboratory, Upton, NY, USA
F. Lin, Oak Ridge National Laboratory, Oak Ridge, TN, USA

Abstract

With the design of the Electron-Ion Collider (EIC) [1], a new Rapid Cycling Synchrotron (RCS) is designed to accelerate the electron bunches from 400 MeV up to 18 GeV. An optimized dynamic aperture with preservation of polarization through the energy ramp was found. The codes DEPOL [2], MADX [3], and BMAD [4] are used in modeling the dynamics and spin preservation. The results will be discussed in this paper.

INTRODUCTION

The EIC will be built at BNL by modifying the Relativistic Heavy Ion Collider (RHIC) [5] existing straight sections. The a new hadron storage ring (HSR) will be built from the arcs of the existing RHIC. The HSR will store polarized protons with energies up 275 GeV and heavy ions up to a beam rigidity of 917 Tm. A new electron storage ring (ESR) [6] has been designed to store electron beams of energies ranging from 5 GeV to 18 GeV. An electron linear accelerator pre-injector will inject a 400 MeV electron beam into the RCS. The RCS, with a circumference ratio to the ESR of approximately 316/315, will accelerate the electron beam to a maximum energy of 18 GeV and will transfer electron bunches to the ESR. Both the RCS and ESR will join the HSR within the existing RHIC tunnel. A schematic of the EIC is seen in Fig. 1.

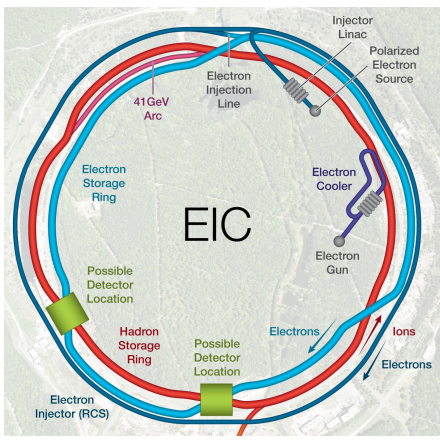

Figure 1: Overhead schematic of EIC electron accelerator.

MAGNETIC LATTICE

The magnetic lattice of the RCS has three distinct sections due to the need for high periodicity [7]. The arcs of the RCS contains four interleaved sextupole families, labeled *sxfa, sxda, sxfb,* and *sxdb*, to correct the chromaticity of a $\pi/2$ phase advance, $\phi_{x,y}$ FODO cell. The RCS has two unique straight section designs. In the 6 o'clock and 8 o'clock regions of the lattice, the dipoles are arranged such that the beam line bypasses the detectors with the lattice centerline 5 m away from the centerline of the tunnel. In both straight section configurations, the magnetic lattice is symmetric about the midpoint. In the 10 o'clock straight section, ten 591 MHz cavities are located split with five cavities on one side of the midpoint and five cavities on the other side of the midpoint. In the experimental bypass straight sections the number of sextupole families is eleven while in the other straights the number of families is four. Figure 2 shows the arrangement of the sextupoles in each of the three lattice sections. Each of the lattice quadrupoles have a effective length of 0.6 m and the sextupole effective length is 0.5 m.

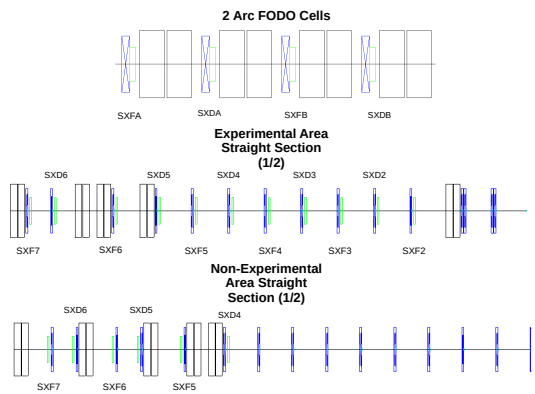

Figure 2: Lattice layout of the arc cells, spin transparent experimental bypasses, and the utility straight sections. Dipoles (black), quadrupoles (blue), and sextupoles (green) are shown. Each straight section is symmetric about the midpoint of the lattice.

OPTICS

The optical design of the RCS was based upon the need to minimized the intrinsic and imperfection depolarization resonances through the energy ramp and to provide at least a 5σ beam envelope that fits within the 32.9 mm diameter beam pipe. Thus, with a 40 mm-mrad injection rms emittance, the $\beta_{max(x,y)}$ is 120 m. The dispersion, η_x, at the center of the non-experimental straight sections was constrained to be zero. Figure 3 shows the β functions, η, and 5σ beam envelopes of the RCS. The fractional tunes, $\nu_{x,y}$, were selected to be far from the half integer and third integer

* hlovelace@bnl.gov

ISBN: 978-3-95450-227-1 ISSN: 2673-5490 doi:10.18429/JACoW-IPAC2022-MOPOST055

resonances. The RCS ramps to energies 5, 10, and 18 GeV decreasing the unnormalized emittance of the electron beam to 4 nm, 2 nm, and 1 nm through adiabatic damping providing a larger dynamic aperture as the γ increases. Since the electron beam emittance is largest and the dynamic aperture is the smallest at injection energy, the optics of the RCS was optimized at 400 MeV. An injected 40 ps rms, 7 nC bunch will merge into 180 ps rms, 28 nC bunch at injection energy, keeping the momentum spread, $\Delta p/p$, at 2.5×10^{-3} rms.

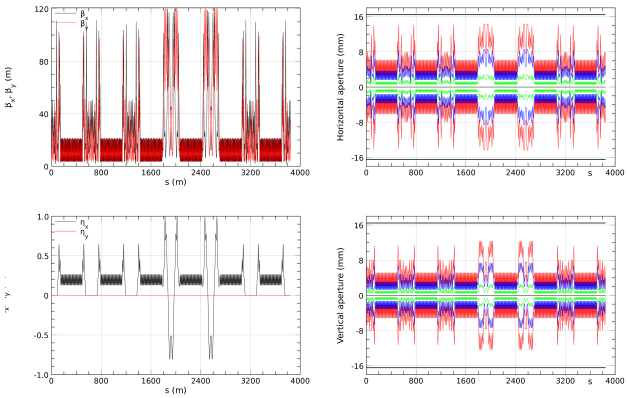

Figure 3: Top left: β functions, bottom left: η, top right: σ_x, bottom right: σ_y. The red curve represents the 5σ beam envelope. Curve start at 12 o'clock straight section and plots clockwise through lattice.

Linear Optics Optimization

Since the RCS ramps a polarized electron beam from 400 MeV to 18 GeV, the optics are design so that the average of normalized strengths of the quadrupoles in the straight sections were minimal which directly minimizes both the imperfection and intrinsic depolarization resonances strengths, ϵ_r:

$$\epsilon_r \propto \sum (k_1 L)_n \tag{1}$$

The constraining normalized strength limit of the RCS quadrupoles is 0.45 T/m^2. The sextupole normalized strength limit is 7 T/m^3. Table 1 lists the RCS parameters.

Nonlinear Optics Optimization

The linear chromaticity, $\xi_{x,y}$ defined as [8]:

$$\xi_{x,y} = \frac{\partial Q_{x,y}}{\partial \delta} = \frac{1}{4\pi} \oint \beta_{x,y}(s)[\mp K_1(s) \pm K_2(s)\eta_x]ds \tag{2}$$

, needed to eliminate head-tail instability in the RCS has been optimized to 1 in both planes. In equation 2, $K_n = \frac{1}{b\rho}\frac{\partial B_y^n}{\partial x^n}|_{x=y=0}$. This chromaticity was selected to minimize the tune spread at injection and throughout the ramp. The chromatic aberrations, $W_{x,y}$ are defined as [9]:

Table 1: List of Selected RCS Parameters

Parameter	Value
Circumference [m]	3846.17
Injection energy [MeV]	400
Top energy [GeV]	18
Normalized emittance [mm-mrad]	40
Momentum compaction α_c	0.00028
Gamma Transition γ_t	59.74
Max relative pol. loss	1%
Ramping repetition rate [Hz]	1
Acceleration time [ms], [turns]	100, 8000
"Spin effective" superperiods	96
No. of quadrupoles	506
No. of sextupoles	422
Arc Cell (^{o}) ϕ_x, ϕ_y	92.52, 94.84
Tune Q_x, Q_y	58.8, 64.2
Natural Chromaticity ξ_x, ξ_y	-91.64, -91.79

$$\begin{aligned} B &= \lim_{\delta\to 0} \frac{\beta_\delta - \beta_0}{\sqrt{\beta_\delta \beta_0}} \times \frac{1}{\delta} \\ A &= \lim_{\delta\to 0} \frac{\alpha_\delta \beta_0 - \alpha_0 \beta_\delta}{\sqrt{\beta_\delta \beta_0}} \times \frac{1}{\delta} \\ W &= \sqrt{A^2 + B^2}. \end{aligned} \tag{3}$$

where δ is $\Delta p/p$ and the α is the Twiss parameter describing the slope of the β function at a given s coordinate. The first order chromatic, h_{20001}, h_{00201}, h_{10002}, the first order geometric, h_{21000}, h_{30000}, h_{10110}, h_{10020}, h_{10200}, and the second order geometric, h_{31000}, h_{40000}, h_{20110}, h_{11200}, h_{20020}, h_{20200}, h_{00310}, h_{00400} resonance driving terms defined by [10] [11] were used for optimization. The h_{22000}, h_{11110}, and h_{00220} terms which drive the amplitude dependent tune shift (ADTS) were also minimized. The objective of the optimization was to minimize $W_{x,y}$ and the effective Hamiltonian, h, simultaneously. First, global minimization through the use of differential evolution algorithm [12], and then local minimization by the Levenberg–Marquardt algorithm [13].

RESULTS

Figure 4 shows a comparison between the optimized sextupole values and the dispersion. The sextupoles with the maximum absolute strengths are located in the arcs of the RCS. The optimization of the $W_{x,y}$, Figure 5, shows the amplitude of the chromatic perturbations with respect to the s position in the lattice. The largest chromatic correction occurs at the match points exiting entering the experimental bypass straight sections with a particle traveling along an increasing s position.

The tune scan, Figure 6, shows the chromatic curve for a given momentum spread. The second order chromaticities

ISBN: 978-3-95450-227-1 ISSN: 2673-5490 doi:10.18429/JACoW-IPAC2022-MOPOST055

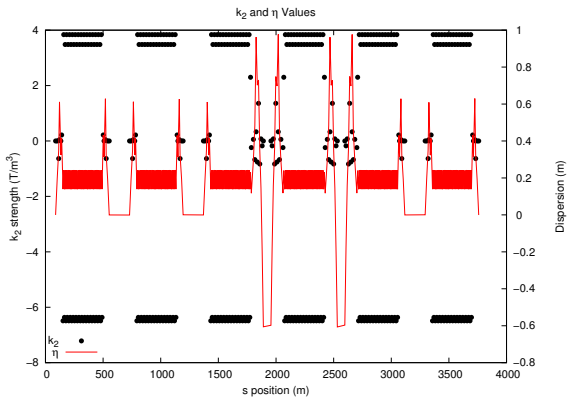

Figure 4: The k_2 value of the sextupole strengths compared to the dispersion function at that s position.

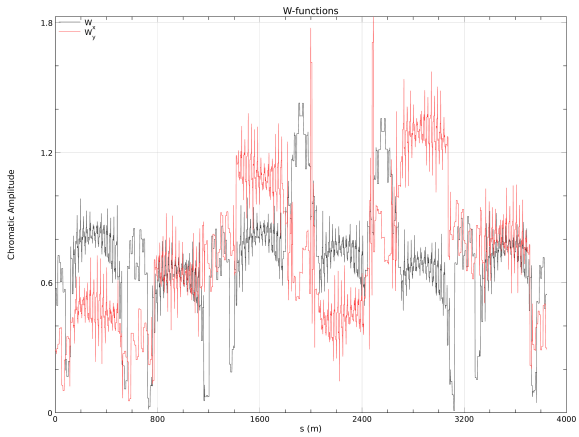

Figure 5: W-functions for the RCS where $\delta = 2.5\times 10^{-3}$.

are $\xi_{2x} = 11.1641$ and $\xi_{2y} = 55.8086$. Third order chromaticities are $\xi_{3x} = 1697.57$ and $\xi_{3y} = 1202.47$. Figure 7, show the strengths of the calculated resonance driving terms.

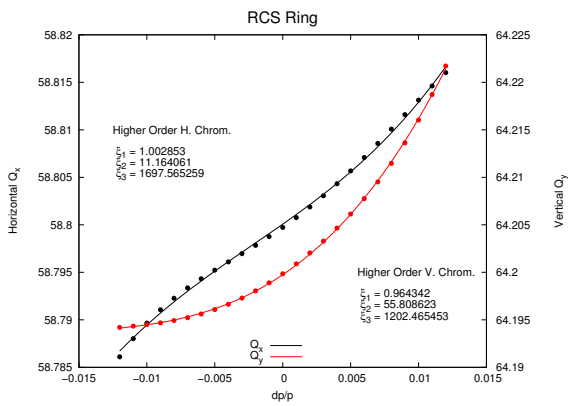

Figure 6: Chromatic Scan of RCS.

The dynamic aperture is shown in Figure 8. The dynamic aperture was taken at the midpoint of 12 o'clock utility straight section at 400 MeV. The β functions at that location are 50.0 m, horizontal, and 3.4 m, vertical. At that location, $\eta_{x,y} = 0$. The dynamic aperture was tracked with a single particle for 10,000 turns using BMAD. For the on momentum particle, a dynamic aperture of 6σ was found. A dynamic aperture of 1σ was found with the $\Delta p/p$ of 1.5% and 0.5σ at -1.5%.

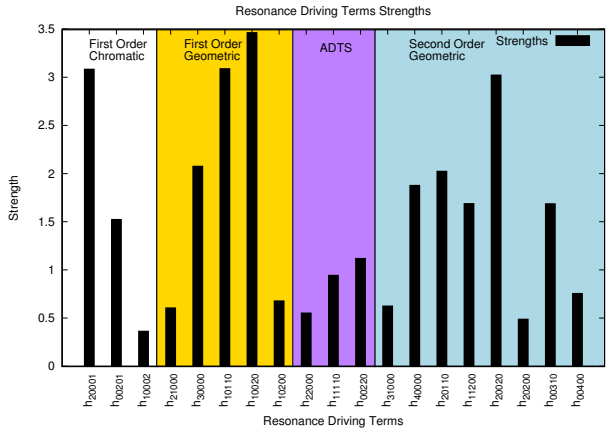

Figure 7: Absolute value of the resonance driving terms strengths. The ADTS were scaled by a factor of 1×10^{-4} and the second order terms were scaled by 1×10^{-3}.

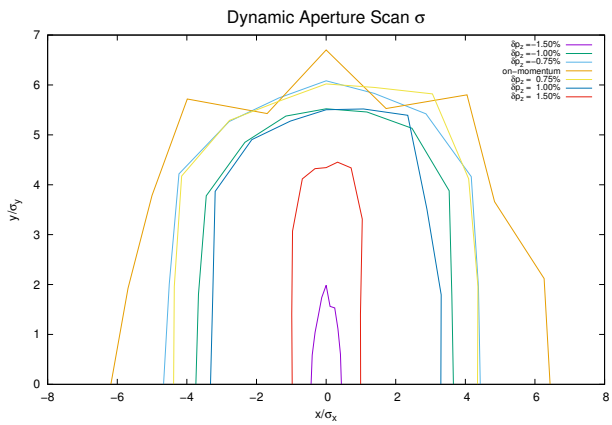

Figure 8: Dynamic Aperture of RCS σ_x=1.6 mm, σ_y=0.4 mm.

CONCLUSION

A dynamic aperture of 6σ at 400 MeV was found for the on-momentum particle of the RCS. The dynamic aperture extends to $\pm$1.5% with a 1σ and 0.5σ, respectively.

ACKNOWLEDGEMENTS

We thank David Sagan for the help in understanding BMAD's dynamic aperture calculation algorithm. We thank the EIC injector group for instructive criticism toward the work presented. Work supported by Brookhaven Science Associates, LLC under Contract No. DE-SC0012704, and Jefferson Science Associates, LLC under Contract No. DE-AC05-06OR23177.

ISBN: 978-3-95450-227-1 ISSN: 2673-5490 doi:10.18429/JACoW-IPAC2022-MOPOST055

REFERENCES

[1] *Electron-Ion Collider at Brookhaven National Laboratory Conceptual Design Report*, EIC collaboration, Collider-Accelerator Department, Upton, NY, 17 ed., October 2020.

[2] Ranjbar, Vahid *et al.* (2004). "Spin coupling resonance and suppression in the AGS". Physical Review Special Topics - Accelerators and Beams. doi:10.1063/1.1607235

[3] H. Grote, F. C. Iselin, "The MAD Program User's Reference Manual", ver. 8.19, CERN/SL/90-13 (AP), Rev. 5, 1996.

[4] D. Sagan, "Bmad: A relativistic charged particle simulation library," *Nucl. Instrum. Meth.*, vol. A558, no. 1, pp. 356–359, 2006. Proceedings of the 8th International Computational Accelerator Physics Conference.

[5] *RHIC:relativistic hadron ion collider con iguration manual*, Accelerator Division, Collider-Accelerator Department, Upton, NY, 4 ed., November 2006.

[6] D. Marx *et al.*, "Designing the EIC Electron Storage Ring Lattice for a Wide Energy Range", presented at IPAC'22, Bangkok, Thailand, Jun. 2022, paper WEPOPT042, this conference.

[7] V. H. Ranjbar, H. Lovelace III, F. Meot, and F. Lin, "EIC's Rapid Cycling Synchrotron Spin Tracking Update", presented at IPAC'22, Bangkok, Thailand, Jun. 2022, paper THPOST004, this conference.

[8] Y. Luo *et al.*, "Sorting Chromatic Sextupoles for Easily and Effectively Correcting Second Order Chromaticity in the Relativistic Heavy Ion Collider", BNL-81976-2009-IR, Brookhaven National Laboratory, 2009↘

[9] B. W. S. L. Montague, "Chromatic effects and their first-order correction", *CAS - CERN Accelerator School: Accelerator Physics*, 1987.

[10] J. Bengtsson, "The Sextupole Scheme for the Swiss Light Source (SLS): An Analytic Approach", Note 9/97, Paul Scherrer Institut., 1997.

[11] Wang, C-X. "Explicit formulas for 2nd-order driving terms due to sextupoles and chromatic effects of quadrupoles". United States. doi:10.2172/1039519

[12] Storn, R., Price, K. "Differential Evolution – A Simple and Efficient Heuristic for global Optimization over Continuous Spaces", *J. of Global Optim.*, vol. 11, pp. 341–359, 1997. doi:10.1023/A:1008202821328

[13] K. Levenberg, "A Method for the Solution of Certain Non-Linear Problems in Least Squares", *Quarterly of Applied Mathematics*, vol. 2, no. 2, 1944, pp. 164–168.